Atmos. Chem. Phys., 13, 4235–4251, 2013
www.atmos-chem-phys.net/13/4235/2013/
doi:10.5194/acp-13-4235-2013

Atmospheric Chemistry and Physics Open Access

Droplet number uncertainties associated with CCN: an assessment using observations and a global model adjoint

R. H. Moore[1,*], **V. A. Karydis**[2], **S. L. Capps**[1], **T. L. Lathem**[2], **and A. Nenes**[1,2]

[1]School of Chemical & Biomolecular Engineering, Georgia Institute of Technology, Atlanta, Georgia, USA
[2]School of Earth & Atmospheric Sciences, Georgia Institute of Technology, Atlanta, Georgia, USA
[*]now at: NASA Postdoctoral Program, NASA Langley Research Center, Hampton, Virginia, USA

Correspondence to: A. Nenes (athanasios.nenes@gatech.edu)

Received: 29 June 2012 – Published in Atmos. Chem. Phys. Discuss.: 16 August 2012
Revised: 18 March 2013 – Accepted: 25 March 2013 – Published: 24 April 2013

Abstract. We use the Global Modelling Initiative (GMI) chemical transport model with a cloud droplet parameterisation adjoint to quantify the sensitivity of cloud droplet number concentration to uncertainties in predicting CCN concentrations. Published CCN closure uncertainties for six different sets of simplifying compositional and mixing state assumptions are used as proxies for modelled CCN uncertainty arising from application of those scenarios. It is found that cloud droplet number concentrations (N_d) are fairly insensitive to the number concentration (N_a) of aerosol which act as CCN over the continents ($\partial \ln N_d / \partial \ln N_a \sim 10$–$30\,\%$), but the sensitivities exceed 70 % in pristine regions such as the Alaskan Arctic and remote oceans. This means that CCN concentration uncertainties of 4–71 % translate into only 1–23 % uncertainty in cloud droplet number, on average. Since most of the anthropogenic indirect forcing is concentrated over the continents, this work shows that the application of Köhler theory and attendant simplifying assumptions in models is not a major source of uncertainty in predicting cloud droplet number or anthropogenic aerosol indirect forcing for the liquid, stratiform clouds simulated in these models. However, it does highlight the sensitivity of some remote areas to pollution brought into the region via long-range transport (e.g., biomass burning) or from seasonal biogenic sources (e.g., phytoplankton as a source of dimethylsulfide in the southern oceans). Since these transient processes are not captured well by the climatological emissions inventories employed by current large-scale models, the uncertainties in aerosol-cloud interactions during these events could be much larger than those uncovered here. This finding motivates additional measurements in these pristine regions, for which few observations exist, to quantify the impact (and associated uncertainty) of transient aerosol processes on cloud properties.

1 Introduction

The ability of atmospheric aerosols to act as cloud condensation nuclei (CCN) remains one of the largest sources of uncertainty in current global climate modelling efforts (Solomon et al., 2007). This is because aerosols are chemically-complex and are derived from a variety of primary emissions sources as well as secondary gas-to-particle conversion in the atmosphere. Given this complexity, there is a need for an extensive global observational dataset that can be used to improve the representation of aerosol-cloud interactions in models.

Measurements of CCN spectra (i.e., CCN concentration over a range of water vapour supersaturation) have been made for decades (e.g., Twomey, 1977; Hudson, 1993, and references therein) and have yielded CCN datasets at a number of locations worldwide. While providing information on the spatiotemporal variation of CCN concentrations and the total particle size distributions, many of these pioneering studies lacked the detailed aerosol composition information needed to fully explain the observed CCN variability. Recent improvements in instrument capabilities have greatly improved the state of the art for measuring the chemical composition and CCN activity of aerosols. This includes the development of the Particle-Into-Liquid Sampler (PILS, Weber et al., 2001) for measuring

water-soluble aerosol composition, the Aerodyne Aerosol Mass Spectrometer (AMS, Jayne et al., 2000; Jimenez et al., 2003) for measuring non-refractory aerosol composition, and the Droplet Measurement Technologies Continuous-Flow, Streamwise, Thermal-Gradient CCN Counter (CCNC, Roberts and Nenes, 2005; Lance et al., 2006) for measuring CCN activation and droplet growth rates. Together with traditional and newer techniques for measuring the aerosol size distribution (e.g., Wang and Flagan, 1989; Flagan, 2004; Cai et al., 2008; Olfert et al., 2008), these robust and commercially-available instruments have enabled a multitude of field studies that have comprehensively characterised the compositional and size dependence of ambient CCN. With this information, it is now possible to empirically evaluate our theoretical understanding of aerosol-cloud interactions using in situ field data.

CCN concentrations are almost exclusively predicted in models with Köhler theory (Köhler, 1936), which has been shown to adequately capture the CCN activity of single- and multi-component aerosol by a large number of laboratory studies (e.g., Cruz and Pandis, 1997; Raymond and Pandis, 2002, 2003; Giebl et al., 2002; Padró et al., 2007). However, atmospheric aerosols are often much more complex than those created in the laboratory, so application of Köhler theory-based models and parameterisations must necessarily make simplifying assumptions regarding the aerosol mixing state and composition in order to reduce their computational burden. To evaluate the uncertainty associated with these simplifying assumptions, a number of "CCN closure" studies have been performed, where the aerosol size distributions and chemical compositions measured in the field are used with the simplifying assumption scenarios to predict CCN number concentrations (N_{CCN}), which are then compared to concurrent CCN measurements with a CCNC. The deviation between the measured and predicted concentrations is interpreted as the uncertainty introduced by that set of simplifying assumptions.

While quantifying the uncertainty in our predictive understanding of CCN concentrations is important, it represents only one link in our understanding of the aerosol-cloud indirect effects on climate. The second link is the combination of CCN concentrations with cloud dynamics (e.g., ambient liquid water content, updraft velocity, and droplet condensational growth rates) to determine the overall cloud droplet concentration (N_d), which, in turn, affects the cloud albedo (A_{cld}) and radiative properties. Studies have combined ambient measurements of N_d with cloud parcel model simulations using measured N_{CCN} and dynamical parameters to perform "cloud droplet closure" (e.g., Hallberg et al., 1997; Chuang et al., 2000; Snider and Brenguier, 2000; Snider et al., 2003; Conant et al., 2004; Meskhidze et al., 2005; Fountoukis et al., 2007). The agreement between predictions and measurements has generally been quite good despite large observed aerosol variability in some studies, with average N_d predicted-to-measured ratios on the order of 0.71–1.2 and some larger ratios reported by Hallberg et al. (1997).

In addition to these field studies, model simulations are an important tool for examining the sensitivity of N_d to changes in CCN and other parameters by selectively turning on and off certain effects. For example, Lance et al. (2004) used a large number of 1-D parcel model simulations to look at the competing influences of aerosol chemistry and cloud updraft velocity in determining N_d under a wide variety of conditions. They found that chemical effects can account for 28–100 % of the variability in N_d for both marine and continental environments. Rissman et al. (2004) extended the droplet parameterisation of Abdul-Razzak et al. (1998) to include the effects of surfactants and derived the analytical sensitivities of N_d with respect to the parameterisation inputs, and reached a similar conclusion that N_d can be up to 1.5-times as sensitive to aerosol composition and surface tension effects as it is to cloud dynamical effects under certain atmospherically relevant conditions. Sotiropoulou et al. (2006) used a droplet parameterisation to propagate the CCN closure uncertainties observed by Medina et al. (2007) during the ICARTT campaign to uncertainties in N_d. Using a campaign-average, prescribed CCN spectrum and size distribution in the parameterisation, they found the uncertainty of N_d to be 50 % of that for N_{CCN} over a range of conditions. Ervens et al. (2010) also modelled the sensitivity of N_d uncertainty to N_{CCN} uncertainty and found that a 100 % overprediction of N_{CCN} leads to only a 15 % overprediction in N_d.

The above studies (and others) highlight the influence of aerosols versus cloud dynamics on cloud properties, and motivates future work with larger scale models to better understand where clouds are most sensitive to aerosol composition effects. Toward this, Sotiropoulou et al. (2007) parameterised the CCN uncertainty from the ICARTT study in terms of supersaturation and used this relationship with the global N_d and N_{CCN} outputs from the NASA Goddard Institute for Space Studies Version II' (GISS II') general circulation model (GCM) to quantify the resulting errors in N_d, aerosol indirect forcing, and autoconversion rate. This is achieved by running two present-day simulations: a base case simulation with normal present day emissions and a perturbed case simulation where the size distribution is varied to alter the CCN concentration according to the ICARTT uncertainty. Their results suggest that a global average CCN prediction error of 10–20 % translates into a 7–14 % uncertainty in N_d and a 10–20 % uncertainty in aerosol indirect forcing (Sotiropoulou et al., 2007). While this study gives important first-order constraints on how CCN uncertainty may affect global indirect forcing estimates, the approach does not account for regional differences in the uncertainty of N_{CCN} or how the model perturbation may induce other, nonlinear effects in the simulation. A thorough discussion of some of these challenges is presented by Lee et al. (2011), who have developed a new statistical method for estimating model sensitivities to input uncertainties and, more recently, used it

to rank parametric uncertainties in cloud droplet formation model parameters (Lee et al., 2013).

There is also a large body of literature related to quantifying aerosol-cloud interactions through correlations of ground-based, airborne and satellite remote sensing measurements. In these studies, the logarithmic sensitivity of N_d to N_a is found through linear regression of *in situ* data or of proxies for N_a such as aerosol optical depth or aerosol index. Reported regression slopes vary widely from 0.1–1.0 (Nakajima and Schulz, 2009; McComiskey and Feingold, 2012, and references therein). Within this wide range, sensitivities over ocean tend to fall within 0.4–0.5 (Nakajima and Schulz, 2009). McComiskey and Feingold (2012) examined how inferred $\partial N_d/\partial N_a$ varied across ground-based, airborne, and satellite platforms, with mean values of 0.48 ± 0.15, 0.58 ± 0.20, and 0.27 ± 0.13 across the different categories of studies, respectively. Low values from satellite-derived measurements were attributed to the effect of aggregating measurement data across scales and not constraining liquid water path in the analysis, which tend to dampen the observed response (McComiskey and Feingold, 2012). The authors note that while this biases inferences of the cloud albedo effect low, it may be more representative of the full aerosol-cloud interactions system, including feedbacks. The sensitivities derived in this work from a physically-based, cloud model parameterisation complement these previous studies by providing a global picture of aerosol-cloud interactions without having to make assumptions with regard to liquid water path constraints; however, given the coarse resolution of the model, this approach does not completely avoid the scale problem discussed by McComiskey and Feingold (2012).

In summary, while there have been several studies to date examining the sensitivity of cloud droplet number concentration uncertainty to uncertainties in CCN number concentration, there is still no clear estimate of the global magnitude of this uncertainty or how it varies regionally. In this study, we address these questions by combining data obtained from over thirty-five published CCN closure studies with simulations conducted with the adjoint of the Kumar et al. (2009) cloud droplet parameterisation, recently developed by Karydis et al. (2012). The adjoint tracks the sensitivity of model output (i.e., N_d) to inputs concurrently with the forward model execution and without perturbing the simulation parameters. Thus, it is able to calculate the sensitivity of N_d to aerosol number concentration, N_a, or a large number of other parameters with analytical precision and requires only a single model run. In the following sections, we briefly discuss the published datasets and the adjoint model before comparing and contrasting the simulation results with observations. The goal of this work is to improve the understanding of the global and regional sensitivities of modelled cloud droplet number to the CCN concentration uncertainty introduced through simplified model assumptions regarding aerosol mixing state and chemical composition. This will inform both future planning of field measurement studies focused on CCN, as well as efforts to quantify model uncertainty and variability.

2 Methods

2.1 CCN uncertainties from aerosol composition and mixing state

In this work, we use CCN prediction uncertainties measured at multiple locations worldwide as a proxy for CCN prediction uncertainty in models employing Köhler theory. Table 1 lists the thirty-six closure study regions considered, which were selected because they involve ambient measurements of CCN concentration, aerosol size distribution, and aerosol chemical composition. Additionally, each reports CCN closure uncertainties for at least one of six common closure scenarios as follows:

1. *Ammonium Sulfate:* all particles are composed of ammonium sulfate with a prescribed Petters and Kreidenweis (2007) hygroscopicity parameter, κ, of 0.6 employed in the Köhler theory calculations.

2. *Internal Mixture, Soluble Organics:* all particles have the same composition as determined by the size-averaged, aerosol composition measurements. Organics are treated as soluble in Köhler theory with a prescribed κ of 0.11, which corresponds to fully-soluble organic material with an average molar mass of 0.2 kg mol^{-1} and density of 1400 kg m^{-3}.

3. *Internal Mixture, Insoluble Organics:* all particles have the same composition as determined by the size-averaged, aerosol composition measurements. Organics are treated as insoluble with $\kappa = 0$.

4. *External Mixture, Soluble Organics:* particles are composed of pure components (e.g., organic particles, ammonium sulfate particles, etc.), and the number of each type is determined by the size-averaged, aerosol composition measurements. Organics are treated as soluble with $\kappa = 0.11$.

5. *External Mixture, Insoluble Organics:* particles are composed of pure components (e.g., organic particles, ammonium sulfate particles, etc.), and the number of each type is determined by the size-averaged, aerosol composition measurements. Organics are treated as insoluble with $\kappa = 0$.

6. *Internal Mixture, Size-Dependent Composition, Insoluble Organics:* particles in each size distribution bin have the same composition as determined by the size-resolved, aerosol composition measurements, but the particle compositions in different size bins may vary. Organics are treated as insoluble with $\kappa = 0$.

Table 1. Summary of past CCN closure studies using measured aerosol compositions and size distributions for predictions.

	Study Location	Dates	GPS Coordinates Latitude	Longitude	Observed N_{CCN} (cm^{-3})	Observed s (%)	Reference
1	Arctic (Alaskan), Spring Background (ARCPAC)	04/2008	65–76° N	130–163° W	100–500	0.1–0.3	Moore et al. (2011)
2	Arctic (N. Atlantic), Summer (ASCOS)	08/2008–09/2008	78–88° N	12° W–16° E	0–200	0.10–0.73	Martin et al. (2011); Paatero et al. (2009)
3	Amazon Rainforest, Brazil (AMAZE–08)	02/2008–03/2008	−3–10° N	50–60° W	40–200	0.10–0.82	Gunthe et al. (2009)
4	Atlanta, GA (AMIGAS)	07/2008–08/2008	33–34° N	84–85° W	500–10 000	0.2–1.0	Padró et al. (2012)
5	Chebogue Point, Canada (ICARTT)	07/2004–08/2004	43–44° N	62–63° W	0–4000	0.65	Ervens et al. (2007, 2010)
6	Canadian Arctic, Summer Background (ARCTAS)	06/2008–07/2008	66–85° N	40–130° W	100–500	0.2–0.57	Lathem et al. (2013)
7	Canadian Arctic, Fresh Biomass Burning (ARCTAS)	06/2008–07/2008	50–57° N	85–120° W	2000–25 000	0.2–0.57	Lathem et al. (2013)
8	Duke Forest, NC (Celtic)	07/2003	34–36° N	75–80° W	0–3000	0.20–0.33	Stroud et al. (2007)
9	Ebert, Ontario, Canada (CARE)	11/2005	43–45° N	79–81° W	400–5000	0.32	Chang et al. (2007)
10	Ebert, Ontario, Canada (CARE)	05/2007–06/2007	43–45° N	79–81° W	0–10 000	0.42	Chang et al. (2010)
11	Finokalia, Greece (FAME-07)	06/2007–10/2007	33–38° N	15–25° E	500–4000	0.21–0.73	Bougiatioti et al. (2009, 2011)
12	Florida Coast (CRYSTAL-FACE)	07/2002	24–27° N	80–84° W	30–6000	0.20–0.85	VanReken et al. (2003)
13	Guangzhou, China (PRIDE-PRD2006)	07/2006	21–24° N	111–115° E	1000–10 000	0.068–0.47	Rose et al. (2011)
14	Gulf Coast, Houston, TX (GoMAACS)	08/2006–09/2006	27–29° N	93–95° W	3000–30 000	0.44	Quinn et al. (2008); Ervens et al. (2010)
15	Gulf of Mexico Background Air (CalNex)	06/2010	27–31° N	84–86° W	100–2500	0.33	Moore et al. (2012b), Unpublished Data
16	Holme Moss, UK	11/2006–12/2006	53–54° N	4–5° W	400–1200	0.30	Ervens et al. (2010)
17	Houston, TX (GoMACCS)	08/2006–09/2006	29–32° N	93–97° W	200–15 000	0.35–1.0	Lance et al. (2009)
18	Houston, TX (TexAQS)	09/2006–10/2006	29–34° N	92–100° W	200–2000	0.30–0.71	Asa-Awuku et al. (2011)
19	Jeju Island, Korea (ABC-EAREX)	03/2005–04/2005	32–36° N	124–128° E	1500–3500	0.6	Yum et al. (2007)
20	Jeju Island, Korea (ABC-EAREX)	03/2005–04/2005	32–36° N	124–128° E	400–4600	0.09–0.97	Kuwata et al. (2008)
21	Jungfraujoch, Switzerland	05/2008	46–47° N	7–9° E	0–1500	0.12–1.18	Jurányi et al. (2010)
22	Los Angeles, CA (CalNex)	05/2010–06/2010	33–35° N	116–118° W	0–7000	0.25–0.65	Moore et al. (2012a)
23	Mexico City, Mexico (MILAGRO)	03/2006	19–20° N	98–100° W	3000–6800	0.29	Wang et al. (2010); Ervens et al. (2010)
24	Monterey, CA (MASE)	07/2005	36–39° N	121–125° W	300–1300	0.1	Ervens et al. (2010)
25	Monterey, CA, Above Cloud (MASE)	07/2005	36–39° N	121–125° W	0–1700	0.2	Wang et al. (2008)
26	Monterey, CA, Marine Boundary Layer (MASE)	07/2005	36–39° N	121–125° W	0–1700	0.2	Wang et al. (2008)
27	Pacific (Eastern), N. California Coast (CIFEX)	04/2004	37–44° N	123–130° W	200–1000	0.2–0.8	Roberts et al. (2006)
28	Pacific (Eastern), Los Angeles, CA (CalNex)	05/2010–06/2010	33–34° N	118–120° W	50–6000	0.25–0.65	Moore et al. (2012a)
29	Riverside, CA (SOAR-I)	07/2005–08/2005	33–34° N	116–119° W	1100–1900	0.27	Cubison et al. (2008); Ervens et al. (2010)
30	San Joaquin Valley, CA (CalNex)	05/2010–06/2010	35–38° N	118–121° W	100–8000	0.25–0.65	Moore et al. (2012a)
31	Sacramento Valley, CA (CalNex)	05/2010–06/2010	38–40° N	121–123° W	50–7000	0.25–0.65	Moore et al. (2012a)
32	Ship Channel, Houston, TX (GoMACCS)	08/2006–09/2006	28–30° N	94–95° W	1400–14 600	0.44	Quinn et al. (2008); Ervens et al. (2010)
33	Ship Exhaust Plume, Monterey, CA (MASE–II)	07/2007	35–36° N	123–124° W	200–30 000	0.10–0.35	Murphy et al. (2009)
34	Southern Great Plains ARM Site, OK	05/2003	35–37° N	96–98° W	100–11 000	2.1–2.8	Rissman et al. (2006)
35	Thompson Farms, NH (ICARTT)	08/2004	42–44° N	70–74° W	100–4000	0.2–0.6	Medina et al. (2007)
36	Toronto, Canada	09/2003	43–44° N	79–80° W	0–3500	0.58	Broekhuizen et al. (2006)

These simplified mixing state and composition assumptions are characteristic of those used in large-scale models to compute CCN concentration and N_d. In another form of CCN closure, some other studies in the literature use the aerosol hygroscopicity obtained from humidified aerosol growth factor measurements to predict CCN concentrations with typically good agreement (e.g., Kim et al., 2011; Kammermann et al., 2010; Vestin et al., 2007; Good et al., 2010; Gasparini et al., 2006; Dusek et al., 2003; Covert et al., 1998, and others). While important for assessing the uncertainties associated with using the same hygroscopicity to predict both subsaturated and supersaturated water uptake, this type of closure study is not included here as it is less relevant for comparing against mass composition-based models.

The studies shown in Table 1 reflect a diverse mixture of urban, rural, and marine sampling on both airborne and ground-based platforms. The majority of published studies focus on locations in North America, and CCN concentrations range from zero to a few thousand particles per cm^3 with the highest concentrations observed in the vicinity of local urban emissions sources (e.g., Houston, TX; Riverside, CA; Mexico City, Mexico) and within targeted biomass burning and ship plumes. Most studies report CCN concentration and closure data at a single or a few discrete supersaturations, and the tabulated values reflect the average across all supersaturations. Since closure results reported in the literature are not described in the same way, we use our judgement in interpreting the closure results described in each study. In many cases the values tabulated in Table 1 reflect an average and standard deviation, while in some studies, the numbers represent the reported mean or median and the total range of observed variability. Given the different uncertainty metrics reported, we do not incorporate these in our analysis in Sect. 3.4. A detailed description of each closure study location, measurements, and data analysis is given by the references in Table 1.

The CCN prediction uncertainties reported by the studies considered are shown in Table 2. Most closure analyses overpredict CCN concentrations. Typically, the external mixing scenarios produce lower predicted CCN concentrations than the ammonium sulfate or internal mixing scenarios. As discussed by Ervens et al. (2010), some studies report large CCN overpredictions on the order of 2–5-fold, which likely reflects the contribution of local emissions sources near the sampling locations that may produce a size-varying, externally-mixed aerosol that cannot be captured well from bulk chemical composition measurements. In some locations (e.g., Houston, TX, and Los Angeles, CA), airborne studies covering a wide horizontal and vertical sampling area report a smaller closure uncertainty than that from ground-based sites in the same area. These conflicting values probably stem from the more local nature of the ground measurements

Table 2. CCN number concentration percent overprediction $(\Delta N_{CCN}/N_{CCN})\times 100\,\%$ for different closure scenarios reported by the studies in Table 1.

			Internal Mixture			External Mixture	
	Study Location	$(NH_4)_2SO_4$	Sol. Org.	Insol. Org.	Size-Dep.	Sol. Org.	Insol. Org.
1	Arctic (Alaskan), Spring Background (ARCPAC)	69±65	57±50	49±47	–	11±30	−23±36
2	Arctic (N. Atlantic), Summer (ASCOS)	–	−6–43±21	–	–	–	–
3	Amazon Rainforest, Brazil (AMAZE-08)	–	14.1	–	–	–	–
4	Atlanta, GA (AMIGAS)	194	157	146	–	169	40
5	Chebogue Point, Canada (ICARTT)	–	40±40	−10±40	–	20±30	−30±30
6	Canadian Arctic, Summer Background (ARCTAS)	–	12±21	−27±16	–	−1±20	–
7	Canadian Arctic, Fresh Biomass Burning (ARCTAS)	–	2±24	−44±16	–	−9±23	–
8	Duke Forest, NC (Celtic)	–	71	20	–	–	–
9	Ebert, Ontario, Canada (CARE)	–	−29	–	-14	–	–
10	Ebert, Ontario, Canada (CARE)	–	–	−3	–	–	–
11	Finokalia, Greece (FAME-07)	–	1.8±12	−2.8±14	−7±11	–	–
12	Florida Coast (CRYSTAL-FACE)	6	–	–	–	–	–
13	Guangzhou, China (PRIDE-PRD2006)	–	20.7	–	–	–	–
14	Gulf Coast, Houston, TX (GoMAACS)	–	130±190	70±100	–	140±190	90±110
15	Gulf of Mexico Background Air (CalNex)	41±26	19±16	13±14	–	5±18	−39±20
16	Holme Moss, UK	–	−10±50	−20±50	–	20±60	0±50
17	Houston, TX (GoMACCS)	36.5	–	2.6	–	–	–
18	Houston, TX (TexAQS)	11.6±9.3	−3.6±7.7	−16.1±10.0	−13.1±8.4	–	−60.9±6.4
19	Jeju Island, Korea (ABC-EAREX)	27±29	–	–	–	–	–
20	Jeju Island, Korea (ABC-EAREX)	16±18	–	–	–	–	–
21	Jungfraujoch, Switzerland	–	4±3	–	–	–	–
22	Los Angeles, CA (CalNex)	84±97	54±57	41±51	18±85	38±49	−16±42
23	Mexico City, Mexico (MILAGRO)	–	10±20	−50±20	10	10±10	−50±20
24	Monterey, CA (MASE)	–	10±60	10±60	–	30±60	30±60
25	Monterey, CA, Above Cloud (MASE)	−54	17	−29	–	−11	−78
26	Monterey, CA, Marine Boundary Layer (MASE)	−8	–	-5	–	–	–
27	Pacific (Eastern), N. California Coast (CIFEX)	79	–	–	–	–	–
28	Pacific (Eastern), Los Angeles, CA (CalNex)	58±90	32±39	23±34	−5±31	20±36	−23±33
29	Riverside, CA (SOAR-I)	–	500±210	360±170	–	390±170	340±180
30	San Joaquin Valley, CA (CalNex)	141±187	71±154	45±126	28±75	56±132	2±67
31	Sacramento Valley, CA (CalNex)	150±190	25±29	−3±26	−14±77	16±25	−59±22
32	Ship Channel, Houston, TX (GoMACCS)	–	320±320	300±300	–	300±300	140±190
33	Ship Exhaust Plume, Monterey, CA (MASE-II)	–	–	23±6	16±6	–	–
34	Southern Great Plains ARM Site, OK	92±192	–	–	–	–	–
35	Thompson Farms, NH (ICARTT)	–	–	35.7±28.5	17.4±27.1	–	–
36	Toronto, Canada	–	–	–	12	–	–
	Number of Studies	16	25	25	11	17	16

versus the regional nature of airborne measurements. To capture the observed range of variability, we evaluate the uncertainties from both sets of measurements, recognising that the former are probably more relevant for finer-scale air quality modelling while the latter are probably more appropriate for comparison with coarser-resolution GCM climate predictions.

2.2 Model description

Simulations were conducted with the NASA Global Modelling Initiative (GMI; http://gmi.gsfc.nasa.gov) chemical transport model (CTM) using offline wind fields and an online aerosol simulation module coupled with the Kumar et al. (2009) droplet activation parameterisation (Karydis et al., 2011). The GMI model is a modular CTM capable of multi-year, global simulations of aerosol concentrations and compositions (Rotman et al., 2001; Considine et al., 2005). The aerosol module used for this study is that of Liu et al. (2005), which uses emissions inputs for SO_2, dimethyl sulfide, H_2O_2, elemental carbon (EC), organic carbon (OC), mineral dust, and sea salt from Liu et al. (2005). The online aerosol module outputs the global distribution of aerosol mass concentrations, which is used to drive the cloud droplet parameterisation and its adjoint.

Before running the offline droplet activation parameterisation, the aerosol mass is first classified as one of four, externally-mixed aerosol modes: fossil fuels (SO_4^{2-}, OC, and EC), biomass burning (OC and EC), marine (SO_4^{2-} and sea salt), and mineral dust. The aerosol within each mode are assumed to be internally mixed and follow a prescribed size distribution as given by Chuang et al. (1997) and Radke et al. (1988) for fossil fuel aerosols, Anderson et al. (1996) for biomass burning aerosols, Lance et al. (2004) for marine aerosols, and d'Almeida (1987) for mineral dust aerosols.

The aerosol number concentration for each type is then computed using these size distributions and a mass fraction-weighted average of the component densities (e.g., SO_4^{2-}, OC, EC) as described in more detail by Karydis et al. (2011).

The aerosol number distributions are then used to drive, offline, a cloud droplet parameterisation (Kumar et al., 2009; Barahona and Nenes, 2007; Fountoukis and Nenes, 2005; Nenes and Seinfeld, 2003) that employs a physically-based method for calculating the aerosol CCN spectrum (i.e., the number of particles that act as CCN as a function of supersaturation) and the maximum supersaturation, s_{max}, for ascending cloud parcels in the global model. The total cloud droplet number, N_d, is then the value of the CCN spectrum at s_{max} in each model grid cell. Recently, the adjoint of the cloud droplet parameterisation has been developed (Karydis et al., 2012), which calculates the sensitivity of N_d to the parameterisation input parameters (i.e, aerosol concentration and composition) during the forward model run. This allows the simultaneous computation of both the mean parameter values and their sensitivities with analytical precision.

2.3 Model application

The model simulation represents a single, climatological year (in this case from March 1997 to February 1998), including a one-month spin up time that is not included in the analysis. This simulated time period was selected to complement the modelling study of Karydis et al. (2011). Meteorological fields were obtained from the GISS II' global climate model (Koch and Rind, 1998; Rind and Lerner, 1996), with a horizontal resolution of 4° latitude by 5° longitude and with 23 vertical layers from surface pressure to 0.01 hPa. The meteorological information in the simulation was updated every three hours. For the droplet parameterisation and its adjoint, a constant effective water uptake coefficient of 0.06 was assumed (Fountoukis et al., 2007), and realistic updraft velocities were prescribed based on observed values for stratocumulus clouds over land ($w = 0.3\,m\,s^{-1}$) and ocean ($w = 0.15\,m\,s^{-1}$) (Chuang et al., 2000; Guibert et al., 2003; Meskhidze et al., 2005). Employing prescribed aerosol properties and cloud updraft velocities for land and ocean introduces additional uncertainty in the model simulations that is not explored in this study, and which may influence the derived sensitivities. The model simulations have been previously evaluated against worldwide observations of cloud droplet number concentrations by Karydis et al. (2011) with reasonably good agreement. Nonetheless, in the next section, we use the observed CCN concentrations reported by the studies in Table 1 to evaluate the ability of the GMI model and emissions inputs to capture this regional variability.

2.4 Model validation

The observed CCN concentrations shown in Table 1 were measured using CCNCs set to prescribed supersaturations ranging from 0.068 % to 2.8 %. In many cases these prescribed supersaturations are higher than predicted in-cloud values, owing to instrument statistical or detection limitations or a desire to probe the CCN activity of Aitken mode particles. This makes it difficult to compare the observed CCN concentrations directly with the modelled droplet concentrations, which correspond to the CCN concentration at $\sim$ 0.1–0.2 % supersaturation. To enable comparison and validate the model against the available CCN dataset, we used the GMI model output with the cloud droplet parameterisation and prescribed supersaturations over the range of experimental values. From the results shown in Table 3, it can be seen that the model is able to predict droplet number concentrations (which in this case is the same as CCN) over the same range as the observed CCN concentrations in 27 of the 36 studies. In nine others, however, the simulated and observed concentration ranges do not overlap and differ by roughly a factor of two (range of -50 % to 69 %). The discrepancies in these locations could be caused by variability in either the aerosol size distribution or number concentration (since s_{max} is known and set equal to the experimental values). Quantifying the uncertainty associated with the model-prescribed size distributions in a meaningful way is not easily accomplished, while the uncertainty due to aerosol loading (derived from emissions uncertainty) is more straightforward. As discussed in the supplementary material, additional simulations were conducted with twice and one-half of the modelled climatological mean aerosol concentration in order to determine how transient aerosol concentrations affect the sensitivities derived in Sect. 3.2. The results suggest that variability in the model aerosol loading introduces a small ($\sim$ 5 %) uncertainty into the following N_d uncertainty analysis.

Our analysis shows that increases in cloud supersaturation tends to increase the derived cloud droplet concentration sensitivity by roughly (14 ± 19) % per 0.1 % supersaturation units. Thus, while the derived sensitivities here are representative of climatologically-relevant stratifrom clouds, they constitute only a lower limit for more strongly-forced, convective clouds.

3 Results and discussion

3.1 Global aerosol concentration (N_a) distributions

The simulated global annual mean aerosol concentration, N_a, is shown in Fig. 1a and is found to be mostly anti-correlated with s_{max} over the continents (not shown), consistent with a pronounced competition for water vapour associated with increases in CCN concentration. The highest concentrations (and lowest s_{max}) are seen over the eastern United States, Europe and east Asia from anthropogenic emissions. Higher concentrations are also predicted for the Southern Hemisphere near and downwind of biomass burning sources.

Table 3. Summary of regional observed CCN number concentration, N_{CCN}; simulated aerosol number concentration, N_a; simulated cloud droplet concentration, N_d; the logarithmic cloud droplet concentration sensitivity, $\left(\frac{\partial ln N_d}{\partial ln N_a}\right)$; and the discrepancy between prediction and observations. Simulations were carried out using a prescribed s_{max} equal to the instrument supersaturation range in each study.

	Study Location	s (%)	Observed N_{CCN} (cm^{-3})	Simulated N_a (cm^{-3})	Simulated N_d (cm^{-3})	$\left(\frac{\partial ln N_d}{\partial ln N_a}\right)$	$(N_d\text{-}N_{CCN})/\max(N_d,N_{CCN})$ Discrepancy (%)
1	Arctic (Alaskan), Spring Background (ARCPAC)	0.1–0.3	100–500	289	90–211	0.650–0.668	
2	Arctic (N. Atlantic), Summer (ASCOS)	0.10–0.73	0–200	–	–	–	
3	Amazon Rainforest, Brazil (AMAZE-08)	0.10–0.82	40–200	1022	184–963	0.340–0.834	
4	Atlanta, GA (AMIGAS)	0.2–1.0	500–10 000	8292	4998–8076	0.612–0.917	
5	Chebogue Point, Canada (ICARTT)	0.65	0–4000	2475	2322	0.858	
6	Canadian Arctic, Summer Background (ARCTAS)	0.2–0.57	100–500	378	219–344	0.662–0.823	
7	Canadian Arctic, Fresh Biomass Burning (ARCTAS)	0.2–0.57	2000–25 000	1086	637–993	0.619–0.830	−50
8	Duke Forest, NC (Celtic)	0.20–0.33	0–3000	7443	4460–5580	0.610–0.697	33
9	Ebert, Ontario, Canada (CARE)	0.32	400–5000	3103	2275	0.690	
10	Ebert, Ontario, Canada (CARE)	0.42	0–10 000	3103	2551	0.749	
11	Finokalia, Greece (FAME-07)	0.21–0.73	500–4000	8167	4179–7423	0.597–0.831	4.3
12	Florida Coast (CRYSTAL-FACE)	0.20–0.85	30–6000	3377	2100–3274	0.612–0.907	
13	Guangzhou, China (PRIDE-PRD2006)	0.068–0.47	1000–10 000	10 503	2556–8833	0.209–0.769	
14	Gulf Coast, Houston, TX (GoMAACS)	0.44	3000–30 000	5960	5037	0.758	
15	Gulf of Mexico Background Air (CalNex)	0.33	100–2500	6741	5,109	0.700	51
16	Holme Moss, UK	0.30	400–1200	6364	3847	0.646	69
17	Houston, TX (GoMACCS)	0.35–1.0	200–15 000	6668	5598–6497	0.757–0.917	
18	Houston, TX (TexAQS)	0.30–0.71	200–2000	5919	4445–5572	0.696–0.862	55
19	Jeju Island, Korea (ABC-EAREX)	0.6	1500–3500	10 649	9481	0.813	63
20	Jeju Island, Korea (ABC-EAREX)	0.09–0.97	400–4600	10 649	2798–10 232	0.203–0.896	
21	Jungfraujoch, Switzerland	0.12–1.18	0–1500	11 408	2263–10 916	0.210–0.893	34
22	Los Angeles, CA (CalNex)	0.25–0.65	0–7000	1786	1222–1635	0.661–0.829	
23	Mexico City, Mexico (MILAGRO)	0.29	3000–6800	4178	3037	0.681	
24	Monterey, CA (MASE)	0.1	300–1300	1435	381	0.327	
25	Monterey, CA, Above Cloud (MASE)	0.2	0–1700	1435	761	0.570	
26	Monterey, CA, Marine Boundary Layer (MASE)	0.2	0–1700	1435	761	0.570	
27	Pacific (Eastern), N. California Coast (CIFEX)	0.2–0.8	200–1000	866	501–821	0.537–0.861	
28	Pacific (Eastern), Los Angeles, CA (CalNex)	0.25–0.65	50–6000	1558	1090–1435	0.657–0.832	
29	Riverside, CA (SOAR-I)	0.27	1100–1900	1670	1184	0.661	
30	San Joaquin Valley, CA (CalNex)	0.25–0.65	100–8000	1710	1142–1554	0.663–0.825	
31	Sacramento Valley, CA (CalNex)	0.25–0.65	50–7000	1435	991–1316	0.651–0.827	
32	Ship Channel, Houston, TX (GoMACCS)	0.44	1400–14 600	5960	5037	0.758	
33	Ship Exhaust Plume, Monterey, CA (MASE-II)	0.10–0.35	200–30 000	1441	411–1153	0.303–0.703	
34	Southern Great Plains ARM Site, OK	2.1–2.8	100–11 000	6313	6290–6304	0.979–0.990	
35	Thompson Farms, NH (ICARTT)	0.2–0.6	100–4000	3723	2099–3371	0.603–0.823	
36	Toronto, Canada	0.58	0–3500	4515	4099	0.826	15

Meanwhile, the lowest concentrations (and highest s_{max} occur in the pristine southern and subtropical oceans and the Alaskan-Canadian Arctic. The simulated global geometric mean aerosol concentration is $502 \overset{\times}{\div} 5.52$ for a mean s_{max} of (0.07 ± 0.03) %.

Simulated N_a and N_d at s_{max} for each of the study locations are given in Table 4. While the s_{max} in these locations is similar to the global average, the simulated N_a and N_d are much higher than the global average due to the past focus on conducting closure studies over the continents. In addition, in some regions, the simulated N_a in Table 4 is considerably less than the maximum observed N_{CCN} given in Tables 1 and 3 (e.g., during Canadian biomass burning, near Houston, TX, and in ship plumes near Monterey, CA). Since N_{CCN} must be less than N_a, these transients show the impact of local emissions sources that are not captured well by the simulated annual mean aerosol concentration. However, as shown in Sect. 2.4, the uncertainty associated with incorrectly modelling these transients is small (~ 5 %).

3.2 Global cloud droplet concentration (N_d) distribution and relative sensitivity of N_d to N_a

Simulated droplet concentrations, N_d, are also shown in Table 4 and in Fig.1b. The global distribution of N_d is similar to that of N_a, but with substantially lower concentrations (approximately five-fold on average). This is shown quantitatively in Fig. 2, as 50–100 % of aerosol form droplets at low concentrations, but the impact on N_d of increasing N_a gradually decreases above $\sim 100\,cm^{-3}$. This implies that the sensitivity of N_d to aerosol depends on the activation fraction, which, in turn, is governed by N_a and s_{max} through the CCN spectrum. Low values of N_a correlate with the highest s_{max} and greatest cloud droplet sensitivity, while the highest N_a correlate with the lowest s_{max} and smallest cloud droplet sensitivity. The sensitivity decreases from 80–90 % at $10\,cm^{-3}$ to nearly zero at 10^4–10^5 cm^{-3}; however, there is no clear trend in s_{max} within this transition region (Fig. 2). This transition arises as aerosol concentration effects become more important than cloud dynamics in determining N_d, and

Table 4. Comparison of regional simulated aerosol number concentration, N_a; simulated cloud droplet concentration, N_d, at s_{max}; the logarithmic cloud droplet concentration sensitivity, $\left(\frac{\partial \ln N_d}{\partial \ln N_a}\right)$; the satellite-derived cloud fraction, f_{cld}; cloud albedo, A_{cld}; and semi-logarithmic albedo sensitivity $\left(\frac{\partial A_{cld}}{\partial \ln N_a}\right)$. Satellite data were obtained from the NASA Giovanni database for CERES and MODIS satellites, as discussed in the text. All reported results are annual arithmetic means (± one standard deviation), except for N_a and N_d, which are geometric means ($\overset{\times}{\div}$ one geometric standard deviation).

	Study Location	Simulated s_{max} (%)	Simulated N_a (cm^{-3})	Simulated N_d (cm^{-3})	$\left(\frac{\partial \ln N_d}{\partial \ln N_a}\right)$	Satellite f_{cld}	Satellite A_{cld}	$\left(\frac{\partial A_{cld}}{\partial \ln N_a}\right)$
1	Arctic (Alaskan), Spring Background (ARCPAC)	0.17	289	147	0.686	0.670	0.497	0.057
2	Arctic (N. Atlantic), Summer (ASCOS)	–	–	–	–	–	–	–
3	Amazon Rainforest, Brazil (AMAZE-08)	0.12	1022	226	0.459	0.660	0.204	0.028
4	Atlanta, GA (AMIGAS)	0.04	8292	612	0.121	0.555	0.400	0.010
5	Chebogue Point, Canada (ICARTT)	0.06	2475	430	0.293	0.723	0.405	0.024
6	Canadian Arctic, Summer Background (ARCTAS)	0.18	378	196	0.669	0.726	0.565	0.055
7	Canadian Arctic, Fresh Biomass Burning (ARCTAS)	0.12	1086	397	0.423	0.662	0.458	0.035
8	Duke Forest, NC (Celtic)	0.04	7443	567	0.156	0.629	0.393	0.012
9	Ebert, Ontario, Canada (CARE)	0.07	3103	520	0.205	0.700	0.449	0.017
10	Ebert, Ontario, Canada (CARE)	0.07	3103	520	0.205	0.700	0.449	0.017
11	Finokalia, Greece (FAME-07)	0.04	8167	392	0.207	0.496	0.352	0.016
12	Florida Coast (CRYSTAL-FACE)	0.04	3377	348	0.295	0.614	0.296	0.020
13	Guangzhou, China (PRIDE-PRD2006)	0.04	10 503	555	0.158	0.713	0.358	0.012
14	Gulf Coast, Houston, TX (GoMAACS)	0.04	5960	434	0.269	0.576	0.356	0.021
15	Gulf of Mexico Background Air (CalNex)	0.04	6741	548	0.172	0.581	0.364	0.013
16	Holme Moss, UK	0.05	6364	378	0.309	0.739	0.419	0.025
17	Houston, TX (GoMACCS)	0.04	6668	496	0.212	0.578	0.374	0.016
18	Houston, TX (TexAQS)	0.04	5919	522	0.192	0.584	0.367	0.015
19	Jeju Island, Korea (ABC-EAREX)	0.04	10 649	472	0.154	0.726	0.380	0.016
20	Jeju Island, Korea (ABC-EAREX)	0.04	10 649	472	0.154	0.726	0.380	0.016
21	Jungfraujoch, Switzerland	0.05	11 408	611	0.116	0.589	0.427	0.009
22	Los Angeles, CA (CalNex)	0.08	1786	346	0.377	0.390	0.359	0.029
23	Mexico City, Mexico (MILAGRO)	0.06	4178	518	0.197	0.649	0.284	0.013
24	Monterey, CA (MASE)	0.08	1435	286	0.416	0.469	0.390	0.033
25	Monterey, CA, Above Cloud (MASE)	0.08	1435	286	0.416	0.469	0.390	0.033
26	Monterey, CA, Marine Boundary Layer (MASE)	0.08	1435	286	0.416	0.469	0.390	0.033
27	Pacific (Eastern), N. California Coast (CIFEX)	0.05	866	126	0.447	0.636	0.361	0.034
28	Pacific (Eastern), Los Angeles, CA (CalNex)	0.07	1558	229	0.418	0.461	0.342	0.031
29	Riverside, CA (SOAR-I)	0.07	1670	288	0.440	0.395	0.326	0.032
30	San Joaquin Valley, CA (CalNex)	0.10	1710	409	0.326	0.442	0.398	0.026
31	Sacramento Valley, CA (CalNex)	0.08	1435	286	0.416	0.470	0.390	0.033
32	Ship Channel, Houston, TX (GoMACCS)	0.04	5960	434	0.269	0.576	0.356	0.021
33	Ship Exhaust Plume, Monterey, CA (MASE-II)	0.06	1441	213	0.491	0.473	0.362	0.038
34	Southern Great Plains ARM Site, OK	0.05	6313	603	0.128	0.574	0.397	0.010
35	Thompson Farms, NH (ICARTT)	0.06	3723	543	0.180	0.443	0.443	0.015
36	Toronto, Canada	0.06	4515	578	0.148	0.440	0.441	0.012
	Mean of All Studies (weighted equally)	0.07±0.04	$3034\overset{\times}{\div}2.57$	$379\overset{\times}{\div}1.51$	0.30±0.15	0.595±0.106	0.386±0.062	0.023±0.012
	Mean of All Studies (weighted by area)	0.09±0.05	$1798\overset{\times}{\div}3.57$	$305\overset{\times}{\div}1.86$	0.38±0.21	0.585±0.101	0.372±0.097	0.027±0.017
	Marine Mean Values	0.06±0.03	$207\overset{\times}{\div}3.72$	$58\overset{\times}{\div}1.81$	0.56±0.18	0.722±0.141	0.291±0.085	0.038±0.016
	Continental Mean Values	0.09±0.04	$2{,}444\overset{\times}{\div}2.90$	$403\overset{\times}{\div}1.67$	0.29±0.19	0.521±0.176	0.355±0.081	0.021±0.014
	Global Mean Values	0.07±0.03	$502\overset{\times}{\div}5.52$	$116\overset{\times}{\div}2.97$	0.46±0.22	0.650±0.173	0.314±0.092	0.032±0.017

occurs around the inflection point of the sigmoidal fit function ($N_a \sim 400\,cm^{-3}$).

As discussed by Karydis et al. (2012), the coarse mode of sea salt aerosol in the model can act as giant CCN (GCCN) in some regions (e.g., the North Atlantic Ocean). GCCN are large enough to activate at very low supersaturations and remove enough water vapour through their condensational growth that the local cloud s_{max} is decreased. This means that fewer droplets can from in the presence of GCCN, resulting in an inverse-Twomey effect and potentially a reduction in shortwave cloud forcing (i.e., $\partial N_d/\partial N_a < 0$). It is difficult to constrain the variability of GCCN, but they likely comprise a negligible fraction of overall measured in situ CCN concentrations. Consequently, for this study, we fix the sea salt partial N_d sensitivity to values greater than or equal to zero (i.e., $\partial N_d/\partial N_{a,seasalt} \geq 0$), noting that the sensitivity may actually become negative in areas with close-to-zero sensitivities in Fig. 1.

The N_d sensitivities shown in Table 4 indicate that most of the closure studies carried out in the past decade have taken place in moderately to heavily-polluted areas, where N_d is weakly sensitive to changes in N_a (~ 10–30 %). Two studies in the Alaskan and Canadian Arctic show lower simulated

Table 5. Percent overprediction of CCN concentration $\left(\frac{\Delta N_{CCN}}{N_{CCN}}\right)$ and simulated cloud droplet concentration $\left(\frac{\Delta N_d}{N_d}\right)$ averaged over the domain of each field study, with equal weighting given to each study location regardless of area. Reported are the mean ± one standard deviation across the 36 different datasets. Since individual field studies do not apply all scenarios, the overprediction values cannot be directly compared; however, the domain-averaged sensitivity ratios $\left(\frac{\Delta N_d}{\Delta N_{CCN}}\right)\left(\frac{N_{CCN}}{N_d}\right)$ are directly comparable, analogous to the sensitivities in Table 4.

Closure Scenario	N	Measured Mean N_{CCN} Overprediction (%)	Simulated Mean N_d Overprediction (%)	$\left(\frac{\Delta N_d}{\Delta N_{CCN}}\right)\left(\frac{N_{CCN}}{N_d}\right)$
$(NH_4)_2SO_4$	16	59±64	18±22	0.31±0.16
Internal Mixture, Soluble Organics (κ_{org} = 0.11)	25	64±118	21±46	0.32±0.16
Internal Mixture, Insoluble Organics (κ_{org} = 0)	25	37±97	12±36	0.33±0.15
Size-Resolved, Internal Mixture, Insoluble Organics (κ_{org} = 0)	11	4±15	1±5	0.29±0.12
External Mixture, Soluble Organics (κ_{org} = 0.11)	17	71±115	23±43	0.37±0.15
External Mixture, Insoluble Organics (κ_{org} = 0)	16	16±104	7±42	0.33±0.14

N_a and higher simulated s_{max} and sensitivity of N_d to N_a ($\sim 70\,\%$). The global mean sensitivity is 0.46 ± 0.22.

Sotiropoulou et al. (2007) simulated global cloud droplet number concentrations and anthropogenic aerosol indirect forcing using the GISS II' GCM and uncovered a similar global mean droplet concentration and geographical distribution as modelled here, but with nearly two-fold lower droplet concentrations in some continental regions. As expected, the spatial pattern of regional aerosol indirect forcing corresponded to the spatial pattern of N_d. Thus, we expect the results of this study to be directly relevant for aerosol indirect forcing estimates even though the direct calculation of aerosol indirect forcing with a radiative transfer model is not performed here.

3.3 Global cloud albedo (A_{cld}) distribution and relative sensitivity of A_{cld} to N_a

The cloud droplet sensitivity discussed in the previous section provides important information regarding the potential sensitivity of clouds in a given region to changes in aerosol concentrations, but it says nothing about whether or not the clouds would form in the first place. This is because global and regional cloudiness is driven by dynamics (e.g., vertical updrafts) and moisture fluxes (e.g., water vapour mixing ratio) in addition to the presence of CCN. Quantifying these individual processes on a global scale is challenging; however, satellite measurements over the past decades have been able to discern global cloudiness with good accuracy. In this study, we use the global annually-averaged cloud albedo (A_{cld}) to capture all of these effects, which is computed as

$$A_{cld} = \frac{A_{tsky} - (1 - f_{cld})A_{csky}}{f_{cld}} \quad (1)$$

where A_{tsky} and A_{csky} are the total sky and clear sky albedos obtained from the NASA CERES mission satellite, respectively, and f_{cld} is the daytime cloud fraction obtained from the MODIS mission satellite. Data were downloaded as annual averages for 2003 from the Giovanni online data system (Acker and Leptoukh, 2007). The global mean cloud albedo is 0.31. A_{cld} directly captures the indirect effect of aerosols on clouds, while f_{cld} indicates the extent to which clouds are present in a given area. The global distributions of A_{cld} and f_{cld} are shown in Fig. 3a and b. Synoptic scale dynamics play a large role in the observed distribution of f_{cld}, with higher cloud fractions seen along the equatorial intertropical convergence zone (ITCZ) and in the mid-latitudes. Meanwhile, the observed cloud fraction is lowest in the subtropical subsidence zones.

In a landmark paper, Twomey (1991) defined the cloud albedo susceptibility to cloud droplet number as (Quaas et al., 2008)

$$\frac{\partial A_{cld}}{\partial N_d} = \frac{A_{cld}\,(1 - A_{cld})}{3N_d} \quad (2)$$

for a constant amount of liquid water and by making a number of simplifying assumptions regarding the radiative properties of liquid water droplets. Equation (2) indicates that A_{cld} is at peak sensitivity to N_d when $A_{cld} = 0.5$, where $\partial A_{cld}/\partial N_d = 1/(12N_d)$.

Combining the satellite-derived $\partial A_{cld}/\partial N_d$ with the model-derived $\partial N_d/\partial N_a$ yields the overall sensitivity of cloud albedo to aerosol concentration, $\partial A_{cld}/\partial N_a$, which is shown scaled by cloud fraction in Fig. 3d. Overall, the spatial distribution of the scaled albedo sensitivity is similar to the cloud droplet number sensitivity, except that the former exhibits decreased sensitivity in the subtropical subsidence zones, where both N_d and cloudiness are low. The most sensitive regions are in the southern oceans and Arctic regions where a doubling of aerosol concentrations can be seen to induce the largest absolute change in albedo. Oreopoulos and Platnick (2008) also uncovered a similar spatial pattern of relative albedo sensitivity using MODIS satellite retrievals coupled with a detailed radiative transfer algorithm. They found distinct seasonal variation with the highest sensitivities found in coastal ocean upwelling zones throughout April–October and in the southern oceans during austral

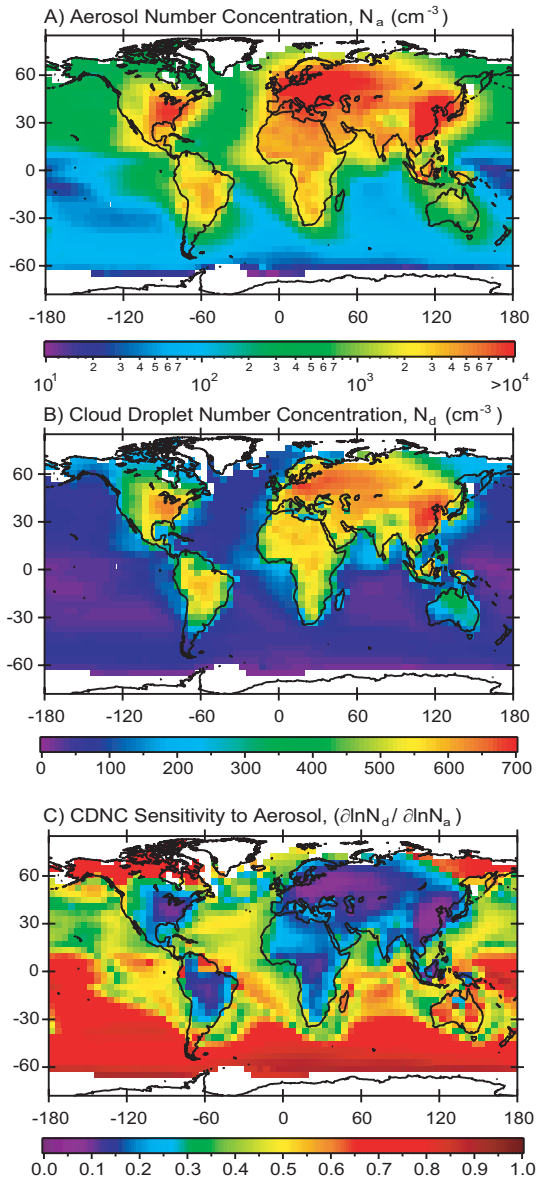

Fig. 1. Simulated global spatial distribution of the annual mean N_a **(A)**, N_d **(B)** and logarithmic sensitivity of N_d to N_a **(C)**.

summer (Oreopoulos and Platnick, 2008). However, it is important to note that the sensitivities presented here do not include the mitigating effects of dynamical feedbacks (e.g., Koren and Feingold, 2011; Stevens and Feingold, 2009). Consequently, while the magnitude of this sensitivity may reflect an upper limit, the spatial distribution shown in Fig. 3d shows the key regions of the world where the sensitivity of cloud properties to aerosol is large.

3.4 Cloud droplet number uncertainties and implications for the indirect effect

In this section, the CCN closure uncertainties from Sect. 2.1 (Table 2) and the modelled cloud droplet sensitivities from Sect. 3.2 (Table 4) are combined to estimate the overall N_d uncertainty arising from simplifying assumptions in Köhler theory that are typically applied in global modelling studies of aerosol-cloud interactions. Figure 4 gives the field measurement uncertainties for five of the six closure scenarios. The left panels show the approximate spatial extent of those study areas located in North America and Europe and are coloured by the N_{CCN} overprediction $\left(\frac{\Delta N_{CCN}}{N_{CCN}}\right)$ from Table 2. The right panels show the estimated N_d overprediction $\left(\frac{\Delta N_d}{N_d}\right)$ calculated as $\frac{\Delta N_d}{N_d} = \left(\frac{\partial N_d}{\partial N_a}\right)\left(\frac{N_a}{N_d}\right)\left(\frac{\Delta N_{CCN}}{N_{CCN}}\right)$. The colour scale for $\frac{\Delta N_{CCN}}{N_{CCN}}$ in Fig. 4 is twice that for $\frac{\Delta N_d}{N_d}$, with light blue denoting zero overprediction (i.e., perfect agreement between Köhler theory predictions and measurements). For most regions in the continental United States and Europe, $\frac{\Delta N_d}{N_d}$ is quite small ($\sim$0–20 %), despite large $\frac{\Delta N_{CCN}}{N_{CCN}}$, which reflects the relative insensitivity of N_d to aerosol concentration uncovered by the model for continental regions (Fig. 1c). Larger $\frac{\Delta N_d}{N_d}$ values are observed in California, in the Alaskan and Canadian Arctic, and in the Amazon rainforest, although only one closure scenario is considered in the Amazon study. In Los Angeles, the large $\frac{\Delta N_d}{N_d}$ reflects the large (nearly five-fold) CCN overprediction reported by Cubison et al. (2008) and Ervens et al. (2010) for all closure scenarios. In the Los Angeles basin and California Central Valley, Moore et al. (2012a) report smaller values of $\frac{\Delta N_{CCN}}{N_{CCN}}$ that vary from -59 to 79 %, and which translate into $\frac{\Delta N_d}{N_d}$ ~ -10–20 %. Reported Arctic CCN uncertainties are considerably lower (Moore et al., 2011), but still have a large effect on $\frac{\Delta N_d}{N_d}$ because of the relatively low modelled droplet concentrations and relatively high modelled N_d sensitivities in pristine regions.

Table 5 shows average uncertainty statistics for the six closure scenarios in this study. These mean values reflect the bias of past closure studies toward locations within the North American continent, which limits their generalisation over the globe. Additionally, the number of studies and the locations of those studies employing each closure scenario are different, which prevents direct cross-scenario comparison. However, the ratio of $\left(\frac{\Delta N_d}{\Delta N_{CCN}}\right)\left(\frac{N_{CCN}}{N_d}\right)$ should be representative of the domain-averaged sensitivities, which can be directly compared despite different sample sizes. We find this ratio to be fairly invariant at 0.29–0.37 for $\frac{\Delta N_d}{N_d}$ $\sim$1–23 %. The N_d uncertainty is consistent with the estimates of N_d sensitivity made by Ervens et al. (2010) ($\sim$15 %) using a parcel model and with average N_d uncertainties of 7–14 % reported by Sotiropoulou et al. (2007) for the United States and Europe. Interestingly, the average N_{CCN} uncertainties reported in the GCM study were also $\sim$10–20 %,

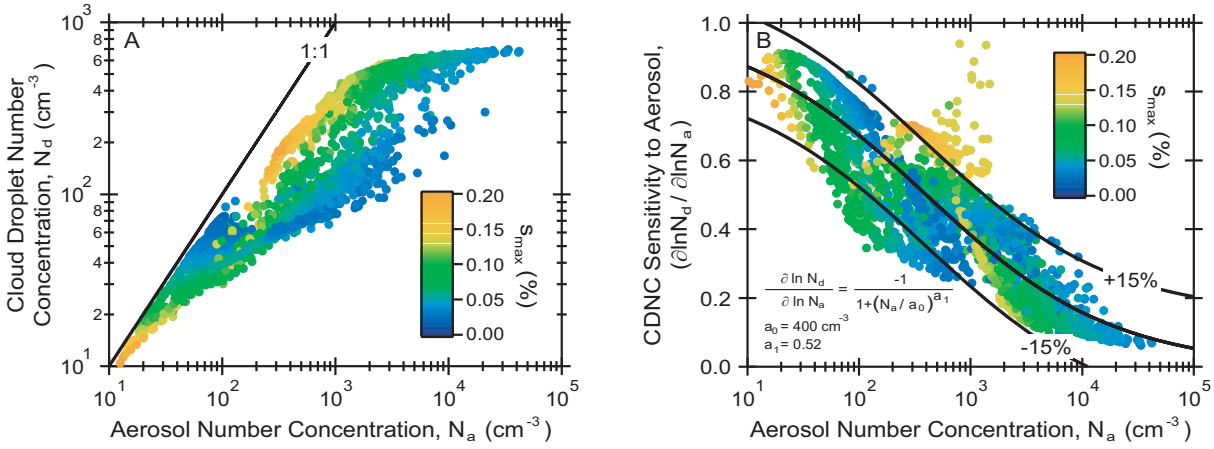

Fig. 2. Simulated N_d (left) and sensitivity of N_d to N_a (right) plotted versus simulated N_a for all grid model grid cells. Each point reflects one grid cell of the global annual mean values shown in Fig. 1, and are coloured by the grid-cell s_{max}.

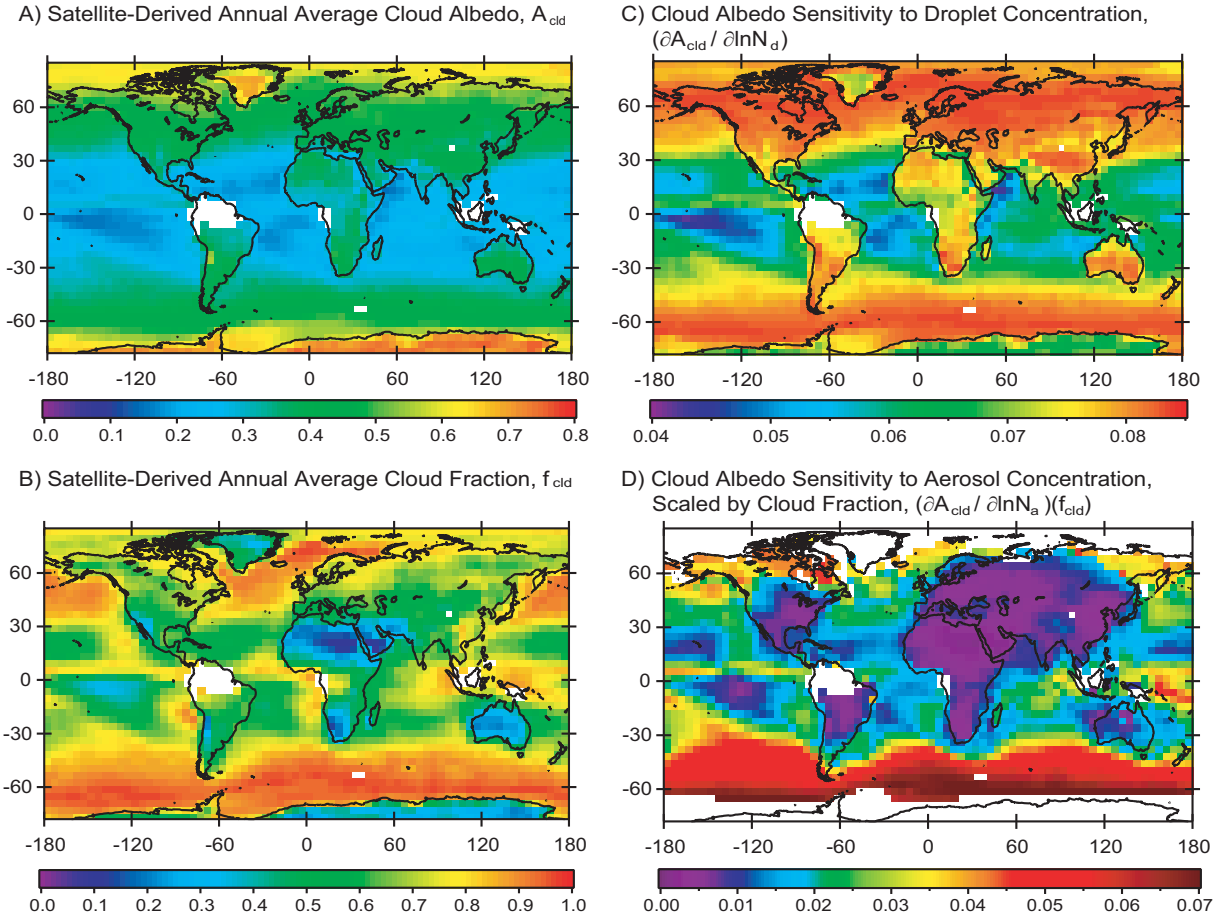

Fig. 3. Global spatial distribution of the annual mean A_{cld} computed from Eq. (1) using NASA CERES satellite data **(A)**, the annual mean MODIS satellite-derived cloud fraction **(B)**, the derived semi-logarithmic sensitivity of A_{cld} to N_d **(C)**, and the derived semi-logarithmic sensitivity of A_{cld} to N_a scaled by cloud fraction **(D)**.

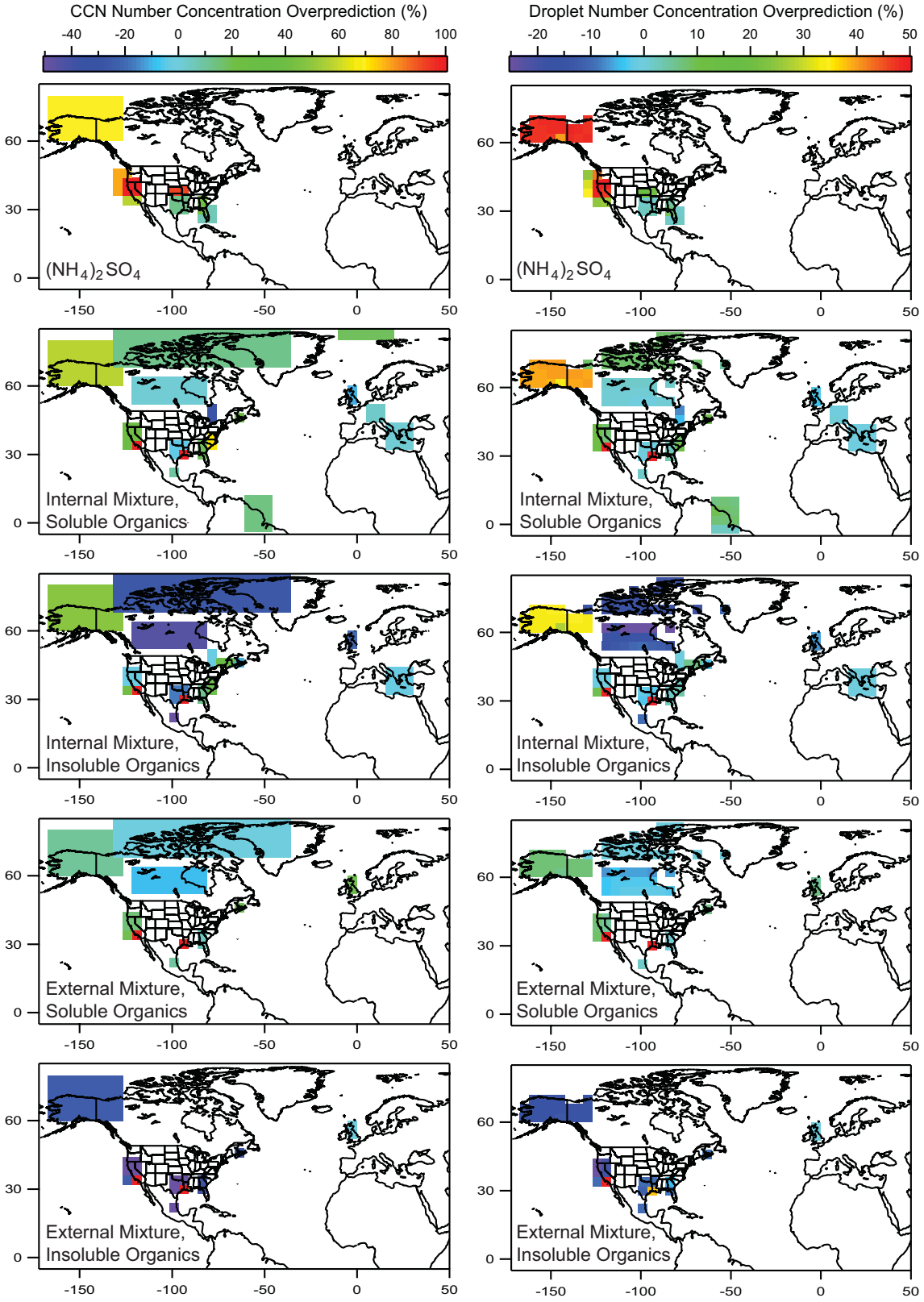

Fig. 4. Regional spatial distribution of measured N_{CCN} uncertainties derived from the closure studies (left) and the N_d uncertainty found by multiplying the measured $\frac{\Delta N_{CCN}}{N_{CCN}}$ by the simulated $\left(\frac{\partial N_d}{\partial N_a}\right)\left(\frac{N_a}{N_d}\right)$ (right).

suggesting a much larger N_d sensitivity than we find here (i.e., $\left(\frac{\Delta N_d}{\Delta N_{CCN}}\right)\left(\frac{N_{CCN}}{N_d}\right) \sim 0.7$ versus the 0.29–0.37 found in this study).

Sotiropoulou et al. (2007) also used the radiative transfer model embedded in the GISS II' GCM to express CCN prediction uncertainty in terms of cloud forcing. They find that a 10–20 % uncertainty in global N_{CCN} results in a 0.1–0.2 W m^{-2} shortwave cloud forcing uncertainty, which is 10–20 % of the anthropogenic indirect effect predicted in the model to be -1.00 W m^{-2}. While this uncertainty is relatively small on a global scale, regional effects are likely to be more substantial. This is especially true when considering larger CCN prediction uncertainties than the range of 10–20 % assumed by Sotiropoulou et al. (2007), and which are suggested by some regional CCN closure studies in Table 2.

4 Summary and conclusions

Modelling simulations conducted with the GMI chemical transport model and cloud parameterisation adjoint are used to interpret and extend the results of thirty-six published CCN closure studies in the literature to estimate the overall uncertainty in cloud droplet number concentration from applying Köhler theory-based parameterisations with simplifying assumptions. We find that the prediction of cloud droplet number is most susceptible to CCN uncertainty at low aerosol concentrations ($N_a < 100$ cm^{-3}) and becomes insensitive to N_{CCN} uncertainty for concentrations above 10^4 cm^{-3}. Thus, pristine areas such as the Arctic and remote oceans are found to be most sensitive (> 70 %), while the sensitivity over continental regions is on the order of 10–30 %, which is consistent with some previous estimates. While the simplifying assumptions employed by past CCN closure studies produce significant overprediction of N_{CCN} when compared to observations, the impact of these uncertainties on the prediction of N_d is on the order of ± 10 % over most of the continental United States, but as high as 30–50 % in the Alaskan Arctic, Houston, TX and Los Angeles, CA, where the highest N_{CCN} prediction uncertainties were observed.

This work shows that the regional sensitivity of N_d to N_{CCN} is important when assessing the uncertainty in cloud droplet number and albedo and, hence, indirect forcing, associated with simplified assumptions regarding CCN. Most CCN closure studies to date have been located in continental regions, and future measurements of CCN and aerosol properties should focus on more remote regions to improve the coverage of the global dataset. Much of the past global anthropogenic indirect forcing has been over the continents, and the results of this study indicate that uncertainties in estimating the global aerosol indirect effect arising from the simplified composition assumptions in models are relatively small. Two questions remain, however, that motivate future research. First, climate models may employ prescribed size distributions for aerosol composition modes, which are likely to be a large source of uncertainty; however, the closure studies employed in this study use measured size distribution information. Consequently, size distribution effects are not reflected in the ΔN_{CCN} proxy. Second, the impact of transient events such as long-range pollution transport or seasonal biogenic emissions sources on changing CCN concentrations remains unclear; the regional sensitivities uncovered in this study indicate that these events may have an important climatic impact. This motivates future field measurements directed at measuring CCN in the southern oceans and Arctic, where observations are limited and seasonal variations have been shown to be significant. These datasets would provide important information to quantify the impact of, and uncertainty associated with, how transient pollution events might influence predictions of CCN concentrations and, hence, clouds and climate.

Supplementary material related to this article is available online at: http://www.atmos-chem-phys.net/13/4235/2013/acp-13-4235-2013-supplement.pdf.

Acknowledgements. RHM acknowledges support from a NASA Postdoctoral Program fellowship and an ESS graduate research fellowship. SLC and TLL also acknowledge support from a NASA ESS graduate research fellowship.

Edited by: M. Kanakidou

References

Abdul-Razzak, H., Ghan, S. J., and Rivera-Carpio, C.: A parameterisation of aerosol activation: 1. Single aerosol type, J. Geophys. Res., 103, 6123–6131, doi:10.1029/97JD03735, 1998.

Acker, J. G. and Leptoukh, G.: Online analysis enhances use of NASA Earth science data, Eos Transactions, 88, 14, doi:10.1029/2007EO020003, 2007.

Anderson, B. E., Grant, W. B., Gregory, G. L., Browell, E. V., James E. Collins, J., Sachse, G. W., Bagwell, D. R., Hudgins, C. H., Blake, D. R., and Blake, N. J.: Aerosols from biomass burning over the tropical South Atlantic region: Distributions and impacts, J. Geophys. Res., 101, 24117–24137, doi:10.1029/96JD00717, 1996.

Asa-Awuku, A., Moore, R. H., Nenes, A., Bahreini, R., Holloway, J. S., Brock, C. A., Middlebrook, A. M., Ryerson, T. B., Jimenez, J. L., DeCarlo, P. F., Hecobian, A., Weber, R. J., Stickel, R., Tanner, D. J., and Huey, L. G.: Airborne cloud condensation nuclei measurements during the 2006 Texas Air Quality Study, J. Geophys. Res., 116, D11201, doi:10.1029/2010JD014874, 2011.

Barahona, D. and Nenes, A.: Parameterization of cloud droplet formation in large-scale models: Including effects of entrainment, J. Geophys. Res., 112, D16206, doi:10.1029/2007JD008473, 2007.

Bougiatioti, A., Fountoukis, C., Kalivitis, N., Pandis, S. N., Nenes, A., and Mihalopoulos, N.: Cloud condensation nuclei measurements in the marine boundary layer of the Eastern Mediterranean: CCN closure and droplet growth kinetics, Atmos. Chem. Phys., 9, 7053–7066, doi:10.5194/acp-9-7053-2009, 2009.

Bougiatioti, A., Nenes, A., Fountoukis, C., Kalivitis, N., Pandis, S. N., and Mihalopoulos, N.: Size-resolved CCN distributions and activation kinetics of aged continental and marine aerosol, Atmos. Chem. Phys., 11, 8791–8808, doi:10.5194/acp-11-8791-2011, 2011.

Broekhuizen, K., Chang, R. Y.-W., Leaitch, W. R., Li, S.-M., and Abbatt, J. P. D.: Closure between measured and modelled cloud condensation nuclei (CCN) using size-resolved aerosol compositions in downtown Toronto, Atmos. Chem. Phys., 6, 2513–2524, doi:10.5194/acp-6-2513-2006, 2006.

Cai, Y., Montague, D. C., Mooiweer-Bryan, W., and Deshler, T.: Performance characteristics of the ultra high sensitivity aerosol spectrometer for particles between 55 and 800 nm: Laboratory and field studies, J. Aerosol Sci., 39, 759–769, doi:10.1016/j.jaerosci.2008.04.007, 2008.

Chang, R. Y.-W., Liu, P. S. K., Leaitch, W. R., and Abbatt, J. P. D.: Comparison between measured and predicted CCN concentrations at Egbert, Ontario: Focus on the organic aerosol fraction at a semi-rural site, Atmos. Environ., 41, 8172–8182, doi:10.1016/j.atmosenv.2007.06.039, 2007.

Chang, R. Y.-W., Slowik, J. G., Shantz, N. C., Vlasenko, A., Liggio, J., Sjostedt, S. J., Leaitch, W. R., and Abbatt, J. P. D.: The hygroscopicity parameter (?) of ambient organic aerosol at a field site subject to biogenic and anthropogenic influences: relationship to degree of aerosol oxidation, Atmos. Chem. Phys., 10, 5047–5064, doi:10.5194/acp-10-5047-2010, 2010.

Chuang, P. Y., Charlson, R. J., and Seinfeld, J. H.: Kinetic limitations on droplet formation in clouds, Nature, 390, 594–596, doi:10.1038/37576, 1997.

Chuang, P. Y., Collins, D. R., Pawlowska, H., Snider, J. R., Jonsson, H. H., Brenguier, J. L., Flagan, R. C., and Seinfeld, J. H.: CCN measurements during ACE-2 and their relationship to cloud microphysical properties, Tellus, 52, 843–867, doi:10.1034/j.1600-0889.2000.00018.x, 2000.

Conant, W. C., VanReken, T. M., Rissman, T. A., Varutbangkul, V., Jonsson, H. H., Nenes, A., Jimenez, J. L., Delia, A. E., Bahreini, R., Roberts, G. C., Flagan, R. C., and Seinfeld, J. H.: Aerosol–cloud drop concentration closure in warm cumulus, J. Geophys. Res., 109, D13204, doi:10.1029/2003JD004324, 2004.

Considine, D. B., Bergmann, D. J., and Liu, H.: Sensitivity of Global Modeling Initiative chemistry and transport model simulations of radon-222 and lead-210 to input meteorological data, Atmos. Chem. Phys., 5, 3389–3406, doi:10.5194/acp-5-3389-2005, 2005.

Covert, D. S., Gras, J. L., Wiedensohler, A., and Stratmann, F.: Comparison of directly measured CCN with CCN modelled from the number-size distribution in the marine boundary layer during ACE 1 at Cape Grim, Tasmania, J. Geophys. Res., 103, 16597–16608, doi:10.1029/98JD01093, 1998.

Cruz, C. N. and Pandis, S. N.: A study of the ability of pure secondary organic aerosol to act as cloud condensation nuclei, Atmos. Environ., 31, 2205–2214, doi:10.1016/S1352-2310(97)00054-X, 1997.

Cubison, M. J., Ervens, B., Feingold, G., Docherty, K. S., Ulbrich, I. M., Shields, L., Prather, K., Hering, S., and Jimenez, J. L.: The influence of chemical composition and mixing state of Los Angeles urban aerosol on CCN number and cloud properties, Atmos. Chem. Phys., 8, 5649–5667, doi:10.5194/acp-8-5649-2008, 2008.

d'Almeida, G. A.: On the variability of desert aerosol radiative characteristics, J. Geophys. Res., 92, 3017–3026, doi:10.1029/JD092iD03p03017, 1987.

Dusek, U., Covert, D. S., Wiedensohler, A., Neusüss, C., Weise, D., and Cantrell, W.: Cloud condensation nuclei spectra derived from size distributions and hygroscopic properties of the aerosol in coastal south-west Portugal during ACE-2, Tellus, 55, 35–53, doi:10.1034/j.1600-0889.2003.00041.x, 2003.

Ervens, B., Cubison, M., Andrews, E., Feingold, G., Ogren, J. A., Jimenez, J. L., DeCarlo, P., and Nenes, A.: Prediction of cloud condensation nucleus number concentration using measurements of aerosol size distributions and composition and light scattering enhancement due to humidity, J. Geophys. Res., 112, D10S32, doi:10.1029/2006JD007426, 2007.

Ervens, B., Cubison, M. J., Andrews, E., Feingold, G., Ogren, J. A., Jimenez, J. L., Quinn, P. K., Bates, T. S., Wang, J., Zhang, Q., Coe, H., Flynn, M., and Allan, J. D.: CCN predictions using simplified assumptions of organic aerosol composition and mixing state: a synthesis from six different locations, Atmos. Chem. Phys., 10, 4795–4807, doi:10.5194/acp-10-4795-2010, 2010.

Flagan, R. C.: Opposed migration aerosol classifier (OMAC), Aerosol Sci. Technol., 38, 890–899, doi:10.1080/027868290505242, 2004.

Fountoukis, C. and Nenes, A.: Continued development of a cloud droplet formation parameterisation for global climate models, J. Geophys. Res., 110, D11212, doi:10.1029/2004JD005591, 2005.

Fountoukis, C., Nenes, A., Meskhidze, N., Bahreini, R., Conant, W. C., Jonsson, H., Murphy, S., Sorooshian, A., Varutbangkul, V., Brechtel, F., Flagan, R. C., and Seinfeld, J. H.: Aerosol-cloud drop concentration closure for clouds sampled during the International Consortium for Atmospheric Research on Transport and Transformation 2004 campaign, J. Geophys. Res., 112, D10S30, doi:10.1029/2006JD007272, 2007.

Gasparini, R., Collins, D. R., Andrews, E., Sheridan, P. J., Ogren, J. A., and Hudson, J. G.: Coupling aerosol size distributions and size-resolved hygroscopicity to predict humidity-dependent optical properties and cloud condensation nuclei spectra, J. Geophys. Res., 111, D05S13, doi:10.1029/2005JD006092, 2006.

Giebl, H., Berner, A., Reischl, G., Puxbaum, H., Kasper-Giebl, A., and Hitzenberger, R.: CCN activation of oxalic and malonic acid test aerosols with the University of Vienna cloud condensation nuclei, Journal of Aerosol Science, 33, 1623–1634, doi:10.1016/S0021-8502(02)00115-5, 2002.

Good, N., Topping, D. O., Allan, J. D., Flynn, M., Fuentes, E., Irwin, M., Williams, P. I., Coe, H., and McFiggans, G.: Consistency between parameterisations of aerosol hygroscopicity and CCN activity during the RHaMBLe discovery cruise, Atmos. Chem. Phys., 10, 3189–3203, doi:10.5194/acp-10-3189-2010, 2010.

Guibert, S., Snider, J. R., and Brenguier, J.-L.: Aerosol activation in marine stratocumulus clouds: 1. Measurement validation for a closure study, J. Geophys. Res., 108, 8628, doi:10.1029/2002JD002678, 2003.

Gunthe, S. S., King, S. M., Rose, D., Chen, Q., Roldin, P., Farmer, D. K., Jimenez, J. L., Artaxo, P., Andreae, M. O., Martin, S. T., and Pöschl, U.: Cloud condensation nuclei in pristine tropical rainforest air of Amazonia: size-resolved measurements and modelling of atmospheric aerosol composition and CCN activity, Atmos. Chem. Phys., 9, 7551–7575, doi:10.5194/acp-9-7551-2009, 2009.

Hallberg, A., Wobrock, W., Flossmann, A. I., Bower, K. N., Noone, K. J., Wiedensohler, A., Hansson, H.-C., Wendisch, M., Berner, A., Kruisz, C., Laj, P., Facchini, M. C., Fuzzi, S., and Arends, B. G.: Microphysics of clouds: Model versus measurements, Atmos. Environ., 31, 2453–2462, doi:10.1016/S1352-2310(97)00041-1, 1997.

Hudson, J. G.: Cloud condensation nuclei, J. Appl. Meteorol., 32, 596–607, doi:10.1175/1520-0450(1993)032¡0596:CCN¿2.0.CO;2, 1993.

Jayne, J. T., Leard, D. C., Zhang, X., Davidovits, P., Smith, K. A., Kolb, C. A., and Worsnop, D. R.: Development of an aerosol mass spectrometer for size and composition analysis of submicron particles, Aerosol Sci. Technol., 33, 49–70, doi:10.1080/027868200410840, 2000.

Jimenez, J. L., Jayne, J. T., Shi, Q., Kolb, C. E., Worsnop, D. R., Yourshaw, I., Seinfeld, J. H., Flagan, R. C., Zhang, X., Smith, K. A., Morris, J. W., and Davidovits, P.: Ambient aerosol sampling using the Aerodyne Aerosol Mass Spectrometer, J. Geophys. Res., 108, 8425, doi:10.1029/2001JD001213, 2003.

Jurányi, Z., Gysel, M., Weingartner, E., DeCarlo, P. F., Kammermann, L., and Baltensperger, U.: Measured and modelled cloud condensation nuclei number concentration at the high alpine site Jungfraujoch, Atmos. Chem. Phys., 10, 7891–7906, doi:10.5194/acp-10-7891-2010, 2010.

Kammermann, L., Gysel, M., Weingartner, E., Herich, H., Cziczo, D. J., Holst, T., Svenningsson, B., Ameth, A., and Baltensperger, U.: Subarctic atmospheric aerosol composition: 3. Measured and modelled properties of cloud condensation nuclei, J. Geophys. Res., 115, D04202, doi:10.1029/2009JD012447, 2010.

Karydis, V. A., Kumar, P., Barahona, D., Sokolik, I. N., and Nenes, A.: On the effect of dust particles on global CCN and cloud droplet number, J. Geophys. Res., 116, D23204, doi:10.1029/2011JD016283, 2011.

Karydis, V. A., Capps, S. L., Russell, A. G., and Nenes, A.: Adjoint sensitivity of global cloud droplet number to aerosol and dynamical parameters, Atmos. Chem. Phys., 12, 9041–9055, doi:10.5194/acp-12-9041-2012, 2012.

Kim, J. H., Yum, S. S., Shim, S., Yoon, S.-C., Hudson, J. G., Park, J., and Lee, S.-J.: On aerosol hygroscopicity, cloud condensation nuclei (CCN) spectra and critical supersaturation measured at two remote islands of Korea between 2006 and 2009, Atmos. Chem. Phys., 11, 12627–12645, doi:10.5194/acp-11-12627-2011, 2011.

Koch, D. and Rind, D.: Beryllium 10/beryllium 7 as a tracer of stratospheric transport, J. Geophys. Res., 103, 3907–3917, doi:10.1029/97JD03117, 1998.

Köhler, H.: The nucleus in and growth of hygroscopic droplets, Transactions of the Faraday Society, 32, 1152–1161, doi:10.1039/TF9363201152, 1936.

Koren, I. and Feingold, G.: Aerosol-cloud-precipitation system as a predator-prey problem, P. Natl. Acad. Sci. USA, 108, 12227–12232, doi:10.1073/pnas.1101777108, 2011.

Kumar, P., Sokolik, I. N., and Nenes, A.: Parameterization of cloud droplet formation for global and regional models: including adsorption activation from insoluble CCN, Atmos. Chem. Phys., 9, 2517–2532, doi:10.5194/acp-9-2517-2009, 2009.

Kuwata, M., Kondo, Y., Miyazaki, Y., Komazaki, Y., Kim, J. H., Yum, S. S., Tanimoto, H., and Matsueda, H.: Cloud condensation nuclei activity at Jeju Island, Korea in spring 2005, Atmos. Chem. Phys., 8, 2933–2948, doi:10.5194/acp-8-2933-2008, 2008.

Lance, S., Nenes, A., and Rissman, T. A.: Chemical and dynamical effects on cloud droplet number: Implications for estimates of the aerosol indirect effect, J. Geophys. Res., 109, D22208, doi:10.1029/2004JD004596, 2004.

Lance, S., Medina, J., Smith, J. N., and Nenes, A.: Mapping the operation of the DMT continuous-flow CCN counter, Aerosol Sci. Technol., 40, 242–254, doi:10.1080/02786820500543290, 2006.

Lance, S., Nenes, A., Mazzoleni, C., Dubey, M. K., Gates, H., Varutbangkul, V., Rissman, T. A., Murphy, S. M., Sorooshian, A., Flagan, R. C., Seinfeld, J. H., Feingold, G., and Jonsson, H. H.: Cloud condensation nuclei activity, closure, and droplet growth kinetics of Houston aerosol during the Gulf of Mexico Atmospheric Composition and Climate Study (GoMACCS), J. Geophys. Res., 114, D00F15, doi:10.1029/2008JD011699, 2009.

Lathem, T. L., Beyersdorf, A. J., Thornhill, K. L., Winstead, E. L., Cubison, M. J., Hecobian, A., Jimenez, J. L., Weber, R. J., Anderson, B. E., and Nenes, A.: Analysis of CCN activity of Arctic aerosol and Canadian biomass burning during summer 2008, Atmos. Chem. Phys., 13, 2735–2756, doi:10.5194/acp-13-2735-2013, 2013.

Lee, L. A., Carslaw, K. S., Pringle, K. J., Mann, G. W., and Spracklen, D. V.: Emulation of a complex global aerosol model to quantify sensitivity to uncertain parameters, Atmos. Chem. Phys., 11, 12253–12273, doi:10.5194/acp-11-12253-2011, 2011.

Lee, L. A., Pringle, K. J., Reddington, C. L., Mann, G. W., Stier, P., Spracklen, D. V., Pierce, J. R., and Carslaw, K. S.: The magnitude and causes of uncertainty in global model simulations of cloud condensation nuclei, Atmos. Chem. Phys. Discuss., 13, 6295–6378, doi:10.5194/acpd-13-6295-2013, 2013.

Liu, X., Penner, J. E., and Herzog, M.: Global modelling of aerosol dynamics: Model description, evaluation, and interactions between sulfate and nonsulfate aerosols, J. Geophys. Res., 110, D18206, doi:10.1029/2004JD005674, 2005.

Martin, M., Chang, R. Y.-W., Sierau, B., Sjogren, S., Swietlicki, E., Abbatt, J. P. D., Leck, C., and Lohmann, U.: Cloud condensation nuclei closure study on summer arctic aerosol, Atmos. Chem. Phys., 11, 11335–11350, doi:10.5194/acp-11-11335-2011, 2011.

McComiskey, A. and Feingold, G.: The scale problem in quantifying aerosol indirect effects, Atmos. Chem. Phys., 12, 1031–1049, doi:10.5194/acp-12-1031-2012, 2012.

Medina, J., Nenes, A., Sotirpoulou, R.-E. P., Cottrell, L. D., Ziemba, L. D., Beckman, P. J., and Griffin, R. J.: Cloud condensation nuclei closure during the International Consortium for Atmospheric Research on Transport and Transformation 2004 campaign: Effects of size-resolved composition, J. Geophys. Res., 112, D10S31, doi:10.1029/2006JD007588, 2007.

Meskhidze, N., Nenes, A., Conant, W. C., and Seinfeld, J. H.: Evaluation of a new cloud droplet activation parameterisation with in situ data from CRYSTAL-FACE and CSTRIPE, J. Geophys. Res., 110, D16202, doi:10.1029/2004JD005703, 2005.

Moore, R. H., Bahreini, R., Brock, C. A., Froyd, K. D., Cozic, J., Holloway, J. S., Middlebrook, A. M., Murphy, D. M., and Nenes, A.: Hygroscopicity and composition of Alaskan Arctic CCN during April 2008, Atmos. Chem. Phys., 11, 11807–11825, doi:10.5194/acp-11-11807-2011, 2011.

Moore, R. H., Cerully, K., Bahreini, R., Brock, C. A., Middlebrook, A. M., and Nenes, A.: Hygroscopicity and composition of California CCN during Summer, 2010, J. Geophys. Res., 117, D00V12, doi:10.1029/2011JD017352, 2012a.

Moore, R. H., Raatikainen, T., Langridge, J. M., Bahreini, R., Brock, C. A., Holloway, J. S., Lack, D. A., Middlebrook, A. M., Perring, A. E., Schwarz, J. P., Spackman, J. R., and Nenes, A.: CCN spectra, hygroscopicity, and droplet activation kinetics of secondary organic aerosol resulting from the 2010 Deepwater Horizon Oil Spill, Environ. Sci. Technol., 46, 3093–3100, doi:10.1021/es203362w, 2012b.

Murphy, S. M., Agrawal, H., Sorooshian, A., Padró, L. T., Gates, H., Hersey, S., Welch, W. A., Jung, H., Miller, J. W., III, D. R. C., Nenes, A., Jonsson, H. H., Flagan, R. C., and Seinfeld, J. H.: Comprehensive simultaneous shipboard and airborne characterisation of exhaust from a modern container ship at sea, Environ. Sci. Technol., 43, 4626–4640, doi:10.1021/es802413j, 2009.

Nakajima, T. and Schulz, M.: Clouds in the Perturbed Climate System, chap. What do we know about large-scale changes of aerosols, clouds, and the radiation budget?, 401–430, MIT Press, 2009.

Nenes, A. and Seinfeld, J. H.: Parameterization of cloud droplet formation in global climate models, J. Geophys. Res., 108, 4415, doi:10.1029/2002JD002911, 2003.

Olfert, J. S., Kulkarni, P., and Wang, J.: Measuring aerosol size distributions with the fast integrated mobility spectrometer, J. Aerosol Sci., 39, 940–956, doi:10.1016/j.jaerosci.2008.06.005, 2008.

Oreopoulos, L. and Platnick, S.: Radiative susceptiblity of cloudy atmospheres to droplet number perturbations: 2. Global analysis from MODIS, J. Geophys. Res., 113, D14S21, doi:10.1029/2007JD009655, 2008.

Paatero, J., Vaattovaara, P., Vestenius, M., Meinander, O., Makkonen, U., Kivi, R., Hyvärinen, A., Asmi, E., Tjernström, M., and Leck, C.: Finnish contribution to the Arctic Summer Cloud Ocean Study (ASCOS) expedition, Arctic Ocean 2008, Geophysica, 45, 119–146, 2009.

Padró, L. T., Asa-Awuku, A., Morrison, R., and Nenes, A.: Inferring thermodynamic properties from CCN activation experiments: single-component and binary aerosols, Atmos. Chem. Phys., 7, 5263–5274, doi:10.5194/acp-7-5263-2007, 2007.

Padró, L. T., Moore, R. H., Zhang, X., Rastogi, N., Weber, R. J., and Nenes, A.: Mixing state and compositional effects on CCN activity and droplet growth kinetics of size-resolved CCN in an urban environment, Atmos. Chem. Phys., 12, 10239–10255, doi:10.5194/acp-12-10239-2012, 2012.

Petters, M. D. and Kreidenweis, S. M.: A single parameter representation of hygroscopic growth and cloud condensation nucleus activity, Atmos. Chem. Phys., 7, 1961–1971, doi:10.5194/acp-7-1961-2007, 2007.

Quaas, J., Boucher, O., Bellouin, N., and Kinne, S.: Satellite-based estimate of the direct and indirect aerosol climate forcing, J. Geophys. Res., 113, D05204, doi:10.1029/2007JD008962, 2008.

Quinn, P. K., Bates, T. S., Coffman, D. J., and Covert, D. S.: Influence of particle size and chemistry on the cloud nucleating properties of aerosols, Atmos. Chem. Phys., 8, 1029–1042, doi:10.5194/acp-8-1029-2008, 2008.

Radke, L. F., Hegg, D. A., Lyons, J. H., Brock, C. A., Hobbs, P. V., Weiss, R., and Rasmussen, R.: Aerosols and Climate, chap. Airborne measurements on smokes from biomass burning, 411–422, Deepak Publishing, 1988.

Raymond, T. M. and Pandis, S. N.: Cloud activation of single-component organic aerosol particles, J. Geophys. Res., 107, 4787, doi:10.1029/2002JD002159, 2002.

Raymond, T. M. and Pandis, S. N.: Formation of cloud droplets by multicomponent organic particles, J. Geophys. Res., 108, 4469, doi:10.1029/2003JD003503, 2003.

Rind, D. and Lerner, J.: Use of on-line tracers as a diagnostic tool in general circulation model development 1. Horizontal and vertical transport in the troposphere, J. Geophys. Res., 101, 12667–12683, doi:10.1029/96JD00551, 1996.

Rissman, T. A., Nenes, A., and Seinfeld, J. H.: Chemical amplification (or dampening) of the Twomey effect: Conditions derived from droplet activation theory, J. Atmos. Sci., 61, 919–930, doi:10.1175/1520-0469(2004)061¡0919:CAODOT¿2.0.CO;2, 2004.

Rissman, T. A., VanReken, T. M., Wang, J., Gasparini, R., Collins, D. R., Jonsson, H. H., Brechtel, F. J., Flagan, R. C., and Seinfeld, J. H.: Characterization of ambient aerosol from measurements of cloud condensation nuclei during 2003 Atmospheric Radiation Measurement Aerosol Intensive Observational Period at the Southern Great Plains site in Oklahoma, J. Geophys. Res., 111, D05S11, doi:10.1029/2004JD005695, 2006.

Roberts, G., Mauger, G., Hadley, O., and Ramanathan, V.: North American and Asian aerosols over the eastern Pacific Ocean and their role in regulating cloud condensation nuclei, J. Geophys. Res., 111, D13205, doi:10.1029/2005JD006661, 2006.

Roberts, G. C. and Nenes, A.: A continuous-flow streamwise thermal-gradient CCN chamber for atmospheric measurements, Aerosol Sci. Technol., 39, 206–221, doi:10.1080/027868290913988, 2005.

Rose, D., Gunthe, S. S., Su, H., Garland, R. M., Yang, H., Berghof, M., Cheng, Y. F., Wehner, B., Achtert, P., Nowak, A., Wiedensohler, A., Takegawa, N., Kondo, Y., Hu, M., Zhang, Y., Andreae, M. O., and Pöschl, U.: Cloud condensation nuclei in polluted air and biomass burning smoke near the mega-city Guangzhou, China – Part 2: Size-resolved aerosol chemical composition, diurnal cycles, and externally mixed weakly CCN-active soot particles, Atmos. Chem. Phys., 11, 2817–2836, doi:10.5194/acp-11-2817-2011, 2011.

Rotman, D. A., Tannahill, J. R., Kinnison, D. E., Connell, P. S., Bergmann, D., Proctor, D., Rodriguez, J. M., Lin, S. J., Rood, R. B., Prather, M. J., Rasch, P. J., Considine, D. B., Ramaroson, R., and Kawa, S. R.: Global Modeling Initiative assessment model: Model description, integration, and testing of the transport shell, J. Geophys. Res., 106, 1669–1691, doi:10.1029/2000JD900463, 2001.

Snider, J. R. and Brenguier, J.-L.: Cloud condensation nuclei and cloud droplet measurements during ACE-2, Tellus, 52, 828–842, doi:10.1034/j.1600-0889.2000.00044.x, 2000.

Snider, J. R., Guibert, S., Brenguier, J.-L., and Putaud, J.-P.: Aerosol activation in marine stratocumulus clouds: 2. Köhler

and parcel theory closure studies, J. Geophys. Res., 108, 8629, doi:10.1029/2002JD002692, 2003.

Solomon, S., Qin, D., Manning, M., Chen, Z., Marquis, M., Averyt, K. B., Tignor, M., and Miller, H. L. (Eds.): Climate Change 2007: The Physical Science Basis, Intergovernmental Panel on Climate Change Fourth Assessment Report, Cambridge University Press, 2007.

Sotiropoulou, R.-E. P., Medina, J., and Nenes, A.: CCN predictions: Is theory sufficient for assessments of the indirect effect?, Geophys. Res. Lett., 33, L05816, doi:10.1029/2005GL025148, 2006.

Sotiropoulou, R.-E. P., Nenes, A., Adams, P. J., and Seinfeld, J. H.: Cloud condensation nuclei prediction error from application of Köhler theory: Importance for the aerosol indirect effect, J. Geophys. Res., 112, D12202, doi:10.1029/2006JD007834, 2007.

Stevens, B. and Feingold, G.: Untangling aerosol effects on clouds and precipitation in a buffered system, Nature, 461, 607–613, doi:10.1038/nature08281, 2009.

Stroud, C. A., Nenes, A., Jimenez, J. L., DeCarlo, P. F., Huffman, J. A., Bruintjes, R., Nemitz, E., Delia, A. E., Toohey, D. W., Guenther, A. B., and Nandi, S.: Cloud activating properties of aerosol observed during CELTIC, J. Atmos. Sci., 64, 441–459, doi:10.1175/JAS3843.1, 2007.

Twomey, S.: The influence of pollution on the shortwave albedo of clouds, J. Atmos. Sci., 34, 1149–1152, doi:10.1175/1520-0469(1977)034¡1149:TIOPOT¿2.0.CO;2, 1977.

Twomey, S.: Aerosols, clouds and radiation, Atmos. Environ., 25, 2435–2442, doi:10.1016/0960-1686(91)90159-5, 1991.

VanReken, T. M., Rissman, T. A., Roberts, G. C., Varutbangkul, V., Jonsson, H. H., Flagan, R. C., and Seinfeld, J. H.: Toward aerosol/cloud condensation nuclei (CCN) closure during CRYSTAL-FACE, J. Geophys. Res., 108, 4633, doi:10.1029/2003JD003582, 2003.

Vestin, A., Rissler, J., Swietlicki, E., Frank, G. P., and Andreae, M. O.: Cloud-nucleating properties of the Amazonian biomass burning aerosol: Cloud condensation nuclei measurements and modelling, J. Geophys. Res., 112, D14201, doi:10.1029/2006JD008104, 2007.

Wang, J., Lee, Y.-N., Daum, P. H., Jayne, J., and Alexander, M. L.: Effects of aerosol organics on cloud condensation nucleus (CCN) concentration and first indirect aerosol effect, Atmos. Chem. Phys., 8, 6325–6339, doi:10.5194/acp-8-6325-2008, 2008.

Wang, J., Cubison, M. J., Aiken, A. C., Jimenez, J. L., and Collins, D. R.: The importance of aerosol mixing state and size-resolved composition on CCN concentration and the variation of the importance with atmospheric aging of aerosols, Atmos. Chem. Phys., 10, 7267–7283, doi:10.5194/acp-10-7267-2010, 2010.

Wang, S. C. and Flagan, R. C.: Scanning electrical mobility spectrometer, J. Aerosol Sci., 20, 1485–1488, doi:10.1016/0021-8502(89)90868-9, 1989.

Weber, R. J., Orsini, D., Daun, Y., Lee, Y.-N., Klotz, P. J., and Brechtel, F.: A particle-into-liquid collector for rapid measurement of aerosol bulk chemical composition, Aerosol Sci. Technol., 35, 718–727, doi:10.1080/02786820152546761, 2001.

Yum, S. S., Roberts, G., Kim, J. H., Song, K., and Kim, D.: Submicron aerosol size distributions and cloud condensation nuclei concentrations measured at Gosan, Korea, during the Atmospheric Brown Clouds–East Asian Regional Experiment 2005, J. Geophys. Res., 112, D22S32, doi:10.1029/2006JD008212, 2007.